

RESEARCH ARTICLE

Single-cell nuclear RNA-sequencing reveals dynamic changes in breast muscle cells during the embryonic development of Ding'an goose

Tieshan Xu^{1,2†}, Yingxiu Hu^{1†}, Haokai Fan^{1,3†}, Xinli Zheng^{1†}, Qicheng Jiang¹, Lizhi Lu⁴, Jie Li⁵, Zhemin Lin¹, Lihong Gu^{1*}

1 Institute of Animal Science & Veterinary Medicine, Hainan Academy of Agricultural Sciences, Haikou, China, **2** Tropical Crop Genetic Resource Research Institute, Chinese Academy of Tropical Agricultural Sciences, Haikou, China, **3** Hainan Institute, Zhejiang University, Yongyou Industry Park, Yazhou Bay Sci-Tech City, Sanya, China, **4** Zhejiang Academy of Agricultural Sciences, Hangzhou, Zhejiang, China, **5** Hainan Wansheng Animal Husbandry Development Co., Ltd, Wanning, China

† These authors contributed equally to this work and should be considered as co-first authors.

* gulihong@hnaas.org.cn



OPEN ACCESS

Citation: Xu T, Hu Y, Fan H, Zheng X, Jiang Q, Lu L, et al. (2025) Single-cell nuclear RNA-sequencing reveals dynamic changes in breast muscle cells during the embryonic development of Ding'an goose. PLoS One 20(12): e0338390. <https://doi.org/10.1371/journal.pone.0338390>

Editor: Mohammad H. Ghazimoradi, Tarbiat Modares University, IRAN, ISLAMIC REPUBLIC OF

Received: August 13, 2025

Accepted: November 23, 2025

Published: December 11, 2025

Copyright: © 2025 Xu et al. This is an open access article distributed under the terms of the [Creative Commons Attribution License](#), which permits unrestricted use, distribution, and reproduction in any medium, provided the original author and source are credited.

Data availability statement: All relevant data are within the paper and its [Supporting Information](#) files.

Funding: This work was supported by China Agriculture Research System of Ministry of Agriculture and Rural Affairs and Ministry

Abstract

Breast muscle is a crucial trait in poultry meat production. Previous studies have identified embryonic day 15 (E15), E21, and E31 as key time points in the breast muscle development of Ding'an goose, yet the specific molecular mechanisms remain unclear. In this study, we analyzed cellular heterogeneity and molecular dynamics at 15th day of embryonic breast muscle of Ding'an goose (E15), E21, and E31 by using single-nucleus RNA-sequencing (snRNA-seq) technology. Nine types of cells were discovered, including fibroblast adipogenic progenitor cells (FAPs), myocytes and muscle stem cells (MuSCs), with notable differences among the three developmental stages in terms of cell type and abundance: FAPs and MuSCs gradually decreased from 42.3% and 35.6% (E15) to 15.7% and 12.2% (E31), respectively, while myocytes increased from 18.5% (E15) to 70.1% (E31). Additionally, the distinct heterogeneity of myocytes, MuSCs and FAPs was determined based on the analysis of gene regulatory networks for each cluster. Developmental trajectory analysis identified genes related to the function and development of MuSCs. The identified differentially expressed genes elucidate the molecular mechanisms of cellular dynamic changes during breast muscle development. This study generated a nuclear profile for single muscle cells that played a key role in the development of breast muscle in Ding'an goose embryos. We investigated metabolic changes at the cellular level during three key developmental stages, thereby refining our understanding of the molecular mechanisms underlying pectoral muscle development specifically in embryonic Ding'an goose.

of Finance [grant number CARS-42-50]. Gu Lihong is the principal investigator of this project and contributed to the supervision and Methodology of this study.

Competing interests: The authors have declared that no competing interests exist.

Abbreviations: DEGs, the differentially expressed genes; FAPs, fibroblast adipogenic progenitor cells/fibroblasts; SCs, Schwann cells; Peri, pericytes; Myocyte, muscle cells; ICs, immune cells; RBCs, red blood cells; ECs, endothelial cells; MuSCs, muscle stem cells; E15, goose the 15th day; E21, goose the 21th day; E31, goose the 31th day.

1. Introduction

Skeletal muscle accounts for approximately 35–60% of body weight in animals [1], which represents a vital trait for the production of poultry meat. Breast muscles are involved in functions such as muscle movement, energy expenditure, and endocrine regulation [2]. Thus, it is a crucial tissue for human and animals. The formation of skeletal muscle involves multiple biological processes such as the proliferation, migration and differentiation of skeletal muscle stem cells, the proliferation and differentiation of myoblasts [3,4]. Almost all muscle fibers have already differentiated and formed during the embryonic stage, and only hypertrophy of muscle fibers and transformation of muscle fiber types occur after birth [5]. Understanding the developmental mechanisms of embryonic breast muscle is therefore crucial for enhancing goose meat yield.

RNA-sequencing (RNA-seq) is widely used to identify regulatory genes in various tissues or organs [6–9], and has significantly promoted the exploration of mechanisms underlying animal economic traits over the past decade. In avian embryonic muscle research, RNA-seq has been applied to screen key regulators in chickens and ducks. For example, studies on broiler chickens identified MYOD1, MYOG and PAX7 as core genes controlling embryonic breast muscle differentiation [10]; in Pekin ducks, RNA-seq analyses linked the Wnt/β-catenin signaling pathway to the proliferation and differentiation of embryonic muscle cells [11]. However, bulk RNA-seq averages transcriptomic signals across cell populations, failing to clearly distinguish changes specific to cell types or subtypes [12], these limitation hinder the study of cell-specific regulatory mechanisms in breast muscle development.

Single-nucleus RNA-sequencing (snRNA-seq) overcomes this drawback by characterizing transcriptomes in the nuclei of individual cells at different developmental stages [13]. This technology enables the analysis of gene expression heterogeneity between cells, the tracking of cell lineage trajectories during development, and the identification of cell-type-specific gene expression [14], making it increasingly widely used in embryonic development research of species such as mice and chickens [15,16]. For instance, snRNA-seq in chicken embryos revealed the heterogeneity of MuSCs and identified subtype-specific regulatory genes during myogenesis [17].

In goose research, however, studies on embryonic breast muscle development remain relatively scarce. Existing studies primarily focus on post-hatch growth. For example, a study on Landes geese found that the mTOR signaling pathway regulates breast muscle hypertrophy by promoting protein synthesis in post-hatch stages [18]; another study on Zhedong white geese explored the relationship between genes related to lipid metabolism and intramuscular fat deposition in post-hatch breast muscle [19]. For embryonic stages, only a few bulk RNA-seq studies have been reported. Our previous study [20] has shown that myogenic differentiation is the major event for the earlier stages and peaks at the 15th day (E15) during the embryonic development of Ding'an goose. After that, the myogenic differentiation slows down, muscle fiber fusion appears and peaks at the 21st day (E21) during the embryonic development of Ding'an goose. With the muscle fiber development of Ding'an goose, it arrives its mature muscle fiber point at the 31st day (E31) during the embryonic development. Thus, E15, E21 and E31 represent three key time points for breast muscle

development, which will provide many key events in the regulation of breast muscle development for Ding'an goose. To date, no studies have applied snRNA-seq to analyze goose embryonic breast muscle, resulting in a lack of understanding of cellular heterogeneity and cell-type-specific regulatory mechanisms during its development.

Ding'an goose is the only local meat goose variety in Hainan Province, and was listed in the National Livestock and Poultry Genetic Resources List in 2010. It has the characteristics of good adaptability, strong stress resistance, high lean meat percentage, and good meat quality, making it an important component of animal husbandry in Hainan Province [20]. To fill the aforementioned research gap, we used snRNA-seq technology to analyze breast muscle cells of Ding'an geese at E15, E21, and E31. The aim of this study is to clarify the dynamic changes and heterogeneity of breast muscle cell populations, and to identify cell-type-specific regulatory genes and pathways, thereby enhancing the understanding of the molecular mechanisms underlying embryonic breast muscle development in Ding'an goose.

2. Methods

2.1. Sample collection

The fertilized eggs of Ding'an goose are provided by Minqiong Poultry Industry Co., Ltd (Hainan, China). All animal experiments were approved by the Animal Ethics Committee of IASVM-HAAS (Approval No.:IASVMHAAS-AE-202489). Fertilized eggs of Ding'an goose were incubated in an incubator at 38°C and 70% relative humidity. At embryonic days 15 (E15), 21 (E21), and 31 (E31), embryos were sacrificed humanely following the AVMA Guidelines for the Euthanasia of Animals (2020).

Embryos were anesthetized via inhalation of 5% isoflurane in oxygen (flow rate: 1 L/min) until the absence of toe-pinch reflex was confirmed. Euthanasia was then performed by cervical dislocation to ensure rapid and painless death. To minimize suffering, all operations were conducted by trained personnel, and embryos were handled gently to avoid unnecessary stress. Incubation and sacrifice procedures were designed to reduce exposure time to non-physiological conditions, and sterile techniques were used during tissue collection to prevent post-mortem contamination.

At the time points of E15, E21, and E31, the breast muscles were aseptically harvested. The left breast muscles were sent to LC Bio Technology Co. Ltd. (Hangzhou, China) for snRNA-seq. Half of the right breast muscles were fixed in 4% paraformaldehyde for immunofluorescence experiments, while the other half were used for fluorescence quantitative PCR experiments. Three individual replicates were set up for each time point.

2.2. Single-nuclei isolation

Nuclei were isolated with Nuclei EZ Lysis buffer (NUC-101; Sigma-Aldrich) supplemented with protease inhibitor (5892791001; Roche) and RNase inhibitor (N2615; Promega and AM2696; Life Technologies). Samples were cut into 1 mm pieces and homogenized using a Dounce homogenizer (885302-0002; Kimble Chase) in 2 ml of ice-cold Nuclei EZ Lysis buffer. They were incubated on ice for 5 minutes with an additional 2 ml of lysis buffer. Grounded with a dounce (Sigma), resuspended by pipette, gently. Incubated on ice for 6 min, then add 2 ml of ice-cold 4% BSA, resuspended by Pasteur pipette, then stop the reaction. Centrifuged at 300g for 5 minutes at 4°C. Add 2 ml of lysis buffer and 4% BSA, resuspended, incubated on ice for 3 min. De-fragment with Miltenyi (Debris Removal Solution). The pellet was resuspended and washed with 4 ml of the buffer, and then, it was incubated on ice for 5 minutes. After another centrifugation. The pellet was resuspended in Nuclei Suspension Buffer (1x PBS, 0.07% BSA, and 0.1% RNase inhibitor). Filtered through a 20-mm cell strainer (43-50020-50; pluriSelect), and counted using a haemocytometer/ Countess II Automated Cell Counter and concentration adjusted to 700–1200 cells/μl.

2.3. Library preparation and sequencing

Single-nuclei suspensions were loaded to 10x Chromium to capture 8000 single cell according to the manufacturer's instructions of 10X Genomics Chromium Single-Cell 3' kit (V3). The following cDNA amplification and library construction

steps were performed according to the standard protocol [21]. Libraries were sequenced on an Illumina NovaSeq 6000 sequencing system (paired-end multiplexing run, 150 bp) by LC-Bio Technology co.ltd., (HangZhou,China) at a minimum depth of 20,000 reads per cell.

2.4 Bioinformatics analysis

First, we used Illumina bcl2fastq software (version 5.01) to multiplex the sequencing results and convert them to FASTQ format. The Cell Ranger pipeline was used for sample demultiplexing, barcode processing, and single-cell 3'-gene counting. Next, snRNA-seq data were aligned with the Ensembl genome goose reference genome, and the Cell Ranger output was loaded into Seurat (version 3.1.1) for dimensionality reduction, clustering, and the analysis of snRNA-seq data [22]. Overall, 25000 cells passed the quality control threshold in that any genes expressed in < 3 cells (default parameter: 1 cell) were removed, the number of genes expressed in each cell > 500 was low, < 5000 was high, the UMI count was < 500, and the percentage of mitochondrial DNA derived gene expression was < 25% [23]. To visualize the data, we used Seurat software to further reduce the dimensionality of all 18339 cells, and t-SNE was used to project the cells into a two-dimensional (2D) space [24]. Then, we used the LogNormalize method in the normalization function of Seurat to calculate gene expression values, and perform principal component analysis on normalized gene expression values. Then, we used cluster and t-SNE analysis to analyze the top 10 principal components [25]. To identify clusters, we selected a clustering method based on a weighted shared nearest neighbor graph. Marker genes for each cluster were identified using the FindAllMarkers function in Seurat and Wilcoxon's rank sum test (default parameter: "bimodal":likelihood ratio test) with default parameters. This process selected marker genes that were expressed in > 10% of cells in the cluster and had a mean log (fold change) > 0.25 (default parameter: 0.26) [26].

2.5. Immunofluorescence staining

The tissues used for immunofluorescence was fixed with an environmentally friendly memory muscle fixative (Servicebio, Hubei, China) for 24 hours. The tissues were dehydrated, embedded, and sectioned for analysis, as described previously [27]. Then, we performed immunohistochemistry with a specific polyclonal antibody (1:200) to detect the spatial distribution of PAX7 (GB113190–50, Servicebio, Hubei, China) protein in skeletal muscle cells, which has been validated in previous studies [28]. Next, we incubated sections with a HRP-labeled secondary antibody (Servicebio, Hubei, China) (1:1000) and counterstained with DAPI (Beyotime, Shanghai, China) (1:1000).

2.6. Fibroblast extraction

For tissues used for fluorescence quantitative PCR, cut them into small pieces with scissors, and digested them with 4% trypsin at 37 °C for one hour. The final cell suspension was then filtered through a 200μm cell filter, centrifuged at 1800 rpm for 10 minutes, washed with PBS, and re-centrifuged for 5 minutes. Adherent cells were collected one hour later.

2.7. Fluorescence quantitative polymerase chain reaction (PCR)

We extracted total RNA from fibroblasts using the Trizol method (Invitrogen, Carlsbad, CA, USA), and measured the concentration of the total RNA with a UV spectrophotometer (A260/280: 1.8–2.0). Then, we used a Tiangen Reverse Transcription Kit (Beijing, China) to synthesize c-DNA for PCR [19]. Primers (Table 1) were designed and synthesized by Shenggong Bioengineering Co., Ltd. (Shanghai, China). GAPDH is widely validated and used as a reference gene in avian muscle development studies [29]. For PCR, we used c-DNA as a template and GAPDH as an internal reference, and fluorescence quantitative PCR system. This allowed us to determine the gene expression by the $2^{-\Delta\Delta Ct}$ method [30]. Three biological replicates and three technical replicates were performed. Experimental data are expressed as mean \pm standard error of the mean. Data were compared with the Student's t-test, and a $P < 0.05$ was considered significant.

Table 1. Primer sequences for real time qPCR.

NCBI number	Gene name	Sequence 5'-3'	Product length (bp)
XM_048079166.2	FOXO3-F	TGCCTTGCCAATTCCATCAGTAAC	117
	FOXO3-R	GAGAGCGGGTCAGAAAGTGTGG	
XM_066995163.1	DCN-F	CTATATCCGTATCGCAGACACCAAC	82
	DCN-R	ACCATCAAGATGAAGTTCGTAAGG	
XM_013172072.3	PLXDC2-F	CCACAGAAGATGACACCAAGATAGC	111
	PLXDC2-R	CAACAATTAAGCCAGCGTGAAGTG	
XM_013178763.3	COL3A1-F	TGGAGAGTCTATGAATGGAGGCTTC	109
	COL3A1-R	GGCACGGCTGGAGAGGATG	
XM_067000417.1	ABLIM1-F	AACCTCTCTCTCCCTGGCTATGG	105
	ABLIM1-R	TCTCTAACACCACCACTCACATCC	
XM_048066782.2	EGFL6-F	TTACCGACTTGCTGGCGAGAG	106
	EGFL6-R	TCCACCTTCATCTTCCCTTTGTTC	
XM_067004670.1	GAPDH-F	GTAGTGAAGGCTGCTGCTGATG	106
	GAPDH-R	CAAAGGTGGAGGAATGGCTGTC	

<https://doi.org/10.1371/journal.pone.0338390.t001>

3. Results

3.1. Identification of different cell types

In order to generate a cell population map for developing breast muscle in goose, we performed snRNA-seq on breast muscle tissues from goose embryos on E15, E21, and E31 (Fig 1a). After Seurat filtering, we collected 18972, 19460, 19843 single cells from E15, E21, and E31 respectively, and resulting in the generation of 26 clusters (Fig 1b). A heatmap showing the top 10 upregulated genes in each of these 26 clusters is presented in Fig 1c, which reveals cluster-specific gene expression patterns that facilitate subsequent cell type annotation. Based on the enriched the differentially expressed genes (DEGs) (Additional file S1 Table) and cell-type specific gene markers in each cluster, nine cell populations were identified (Fig 1d), including fibroblast adipogenic progenitor cells/fibroblasts (FAPs, clusters 2, 7, 12, 13, 18, and 25; Marker genes: PDGFR α , CD34), Schwann cells (SCs, cluster 23; Marker gene: MPZ), pericytes (Peri, clusters 9 and 21; Marker gene: PDGFR β), muscle cells (Myocyte, clusters 1, 4, 5, 6, 19, and 22 Marker genes: MYOD1, MYH1), immune cells (ICs, cluster 16; Marker gene: CD45), red blood cells (RBCs, cluster 17; Marker gene: HBB), endothelial cells (ECs, clusters 14 and 24; Marker gene: CD31), muscle stem cells (MuSCs, clusters 0, 3, 8, 10, 11, and 15; Marker gene: PAX7), and mesenchymal stem cells (cluster 20; Marker gene: CD73). The distributions of cells expressing characteristic gene markers were shown in Fig 1e. In addition, we identified key differences in the abundance of cell clusters for E15, E21, and E31 (Fig 1f). FAPs/fibroblasts, MuSCs, and myocytes were the main constituent cells of breast muscle (over 85%) at three time points. As time progressed, the proportion of FAPs/fibroblasts and MuSCs were decreased (from 35% to 8% and 55% to 20%, respectively), while the proportion of myocytes is increased (from 5% to 70%). For E31, myocytes accounted for the largest cell proportion among the nine cell types (70%). To verify the sequencing results, we conducted immunofluorescence experiments and found that the proportion of MuSCs was consistent with the snRNA-seq results (Fig 1g and Fig 1h). We used qPCR to investigate the expression levels of certain DEGs in fibroblasts and found that the qPCR results were consistent with that of snRNA-seq data (Fig 1i), thus demonstrating the reliability of our sequencing results. Considering the proportion of composition and developmental trends in breast muscles, we further analyzed FAPs/fibroblasts, MuSCs, and myocytes.

3.2. Transcriptional heterogeneity of MuSCs

To investigate the heterogeneity of MuSC, we divided MuSC into 12 clusters and further analysis revealed these cell clusters exhibited characteristics of four main cell sub-types (Fig 2a), including MuSC-0, MuSC-1, MuSC-2, and MuSC-3

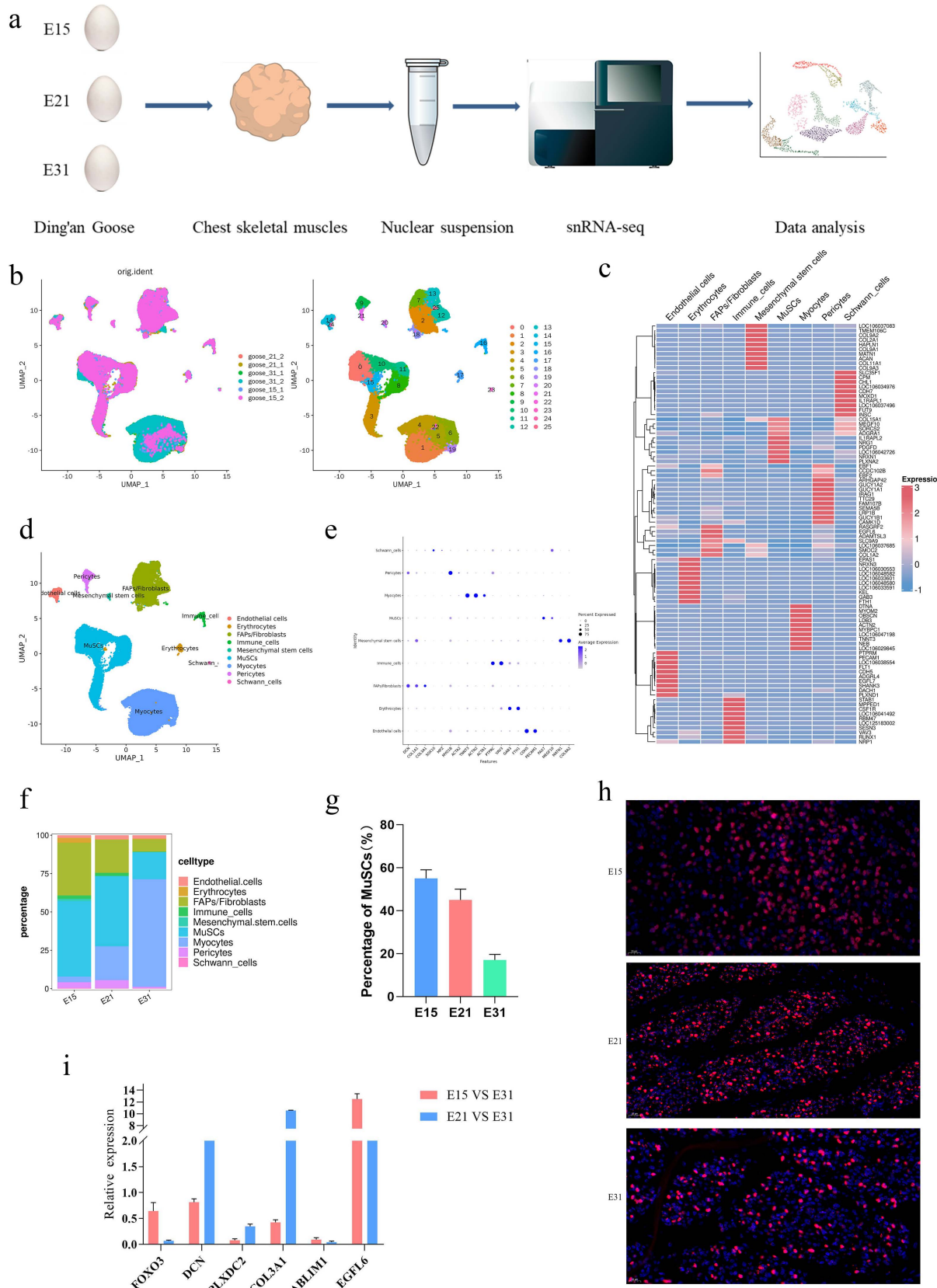


Fig 1. Analysis of different cell types in the breast muscle of goose. (a) Single-cell nuclear sequencing process. (b) 64852 single-cell reduced dimensional maps based on T-distribution random neighborhood embedding (t-SNE), with different colors representing different cell clusters (the same color system applies for all other Figs). (c) Heat map showing the top ten upregulated genes in each cell cluster. (d) t-SNE map of cells identified in the breast muscle. (e) t-SNE plot showing the expression of marker genes in fibroblast adipogenic progenitor cells, Schwann cells, pericytes, myocytes, immune cells, red blood cells, endothelial cells, MuSCs, and mesenchymal stem cells. (f) Proportional diagram showing cells at different developmental stages. (g) Immunofluorescence staining of MuSCs, blue staining (DAPI) represents all cell nuclei, and red staining (PAX7) represents myoblasts. (h) Staining analysis of MuSC immunofluorescence. (i) qPCR analysis of the expression levels of certain DEGs in fibroblasts. Error bars represent the standard error of the mean (SEM); n=3 biological replicates, with 3 technical replicates per biological replicate, the same below.

<https://doi.org/10.1371/journal.pone.0338390.g001>

([Fig 2b](#)). Next, we identified four MuSC sub-groups by characteristic genes ([Fig 2c](#)). MuSC-0 expressed higher levels of *TOP2A*, *MKI67*, and *CENPE*, indicating that the cell population was probably in a proliferative state. Genes related to cell migration, such as *MMP16*, *LAMA4*, and *SRGAP1*, were highly expressed in the MuSC-1. However, the MuSC-2 expressed higher levels of *SOX13*, *PCDH15*, *TEAD4*, and *FILIP1*. The MuSCs-3 cell cluster specifically expressed *ZBTB16*, *FOXO3*, and *COL4A5*. To further reveal the functionality of each MuSC sub-group, we performed functional enrichment for each MuSC sub-group ([Fig 2d](#)). Gene ontology (GO) analysis revealed enrichment in cell division, chromosome separation, and DNA binding in the MuSC-0 cell cluster. The MuSC-1 cluster was enriched in protein binding, signal transduction, and cell migration. The MuSC-2 cluster was associated with the transcriptional regulation of polymerase II and zinc ion binding while the MuSC-3 cluster was associated with protein binding and DNA binding transcription factor activity. Collectively, these results indicated that the transcriptional profiles of different subgroups of MuSCs undergo key changes during the development of embryonic breast muscle in goose, suggesting that they may serve different functions.

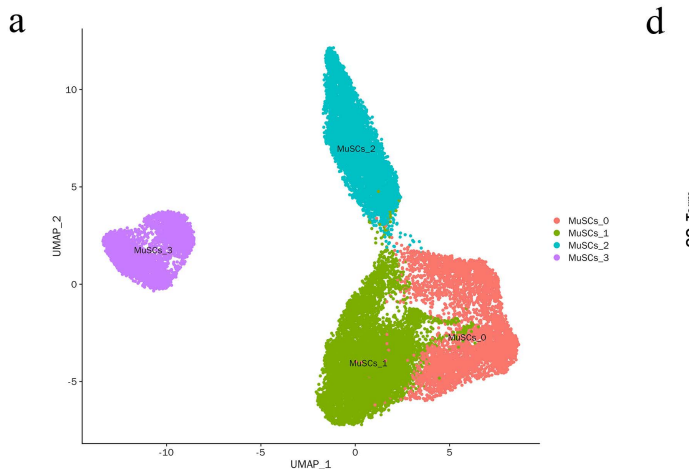
3.3. The transition trajectory of MuSCs

In order to determine the developmental trajectory of MuSCs, we next performed pseudo-time analysis on all MuSC data using clusters based on the Monocle2 algorithm. The differentiation trajectory of MuSCs is shown in [Fig 3a](#). As differentiation progressed, the MuSCs were classified into five states ([Fig 3b](#)), with distinct differentiation trajectories among subgroups and different developmental trajectories ([Fig 3c](#) and [S1 Table](#)). The cell sub-types in the early developmental stage were mainly composed of MuSC-0, while in the middle and late stages were predominantly MuSC-1, MuSC-2, and MuSC-3. In addition, we found that the cell sub-types at E15 were predominantly MuSC-0 and MuSC-1, MuSC-1 and MuSC-2 predominated at E21, and E31 was predominantly MuSC-3 ([Fig 3d](#)).

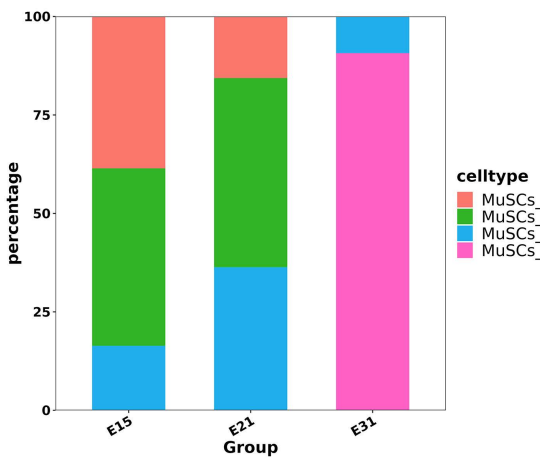
To further investigate the molecular mechanisms underlying the functional evolution of MuSCs, we used BEAM analysis to differentiate the identified branch specific DEGs and observed significant changes in the pseudo time function. According to pseudo-temporal expression patterns, genes were divided into five states ([Fig 3e](#) and [3f](#)). Biological process analysis ([Fig 3g](#)) revealed that genes with high expression of States 1 and 2 were enriched in processes in the cytoplasm and nucleus, while State 3 was associated with cytoplasm and membrane components.

3.4. Typing of FAPs during embryonic development

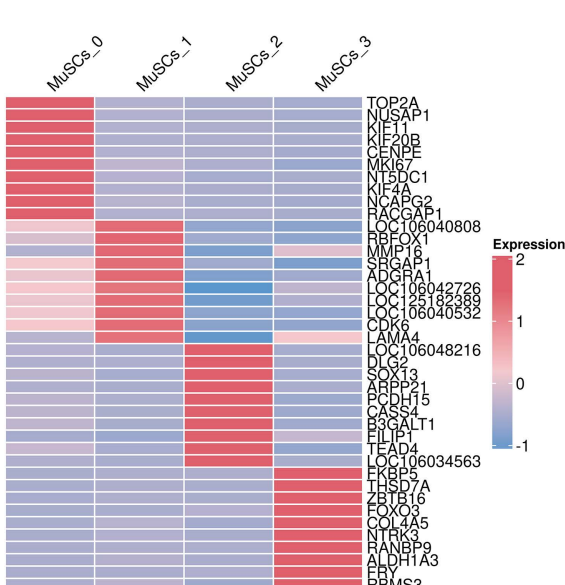
FAPs were divided into 13 clusters, and further analysis revealed that these cell clusters exhibited the characteristics of six main cell sub-types ([Fig 4a](#)), including FAPs-1, FAPs-2, FAPs-3, FAPs-4, FAPs-5, and muscle cell-like FAPs. FAPs-1 upregulated genes ([Fig 4b](#)) were mainly associated with the functionality of extracellular vesicles, cell membranes, and nuclei ([Fig 4c](#)), and also related to ribosomes and metabolic pathways ([Fig 4d](#)), in which they are known to participate in the cell cycle regulation of *EGFL6* overexpression [21]. FAPs-1 was closely related to cell proliferation and development. FAPs-2 upregulated genes were associated with several components, including the cytoplasm, membranes, and protein binding, and were enriched in endocytosis, metabolism, and MAPK signaling pathways. Of these, C-type lectin chondroitin lectin (*CHODL*) was clearly upregulated [22]. The main enrichment of muscle cell-like FAPs was in the nucleus and



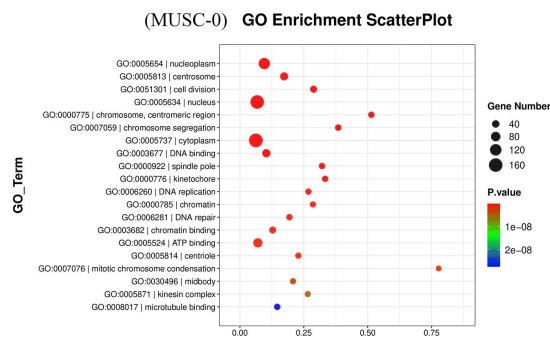
b



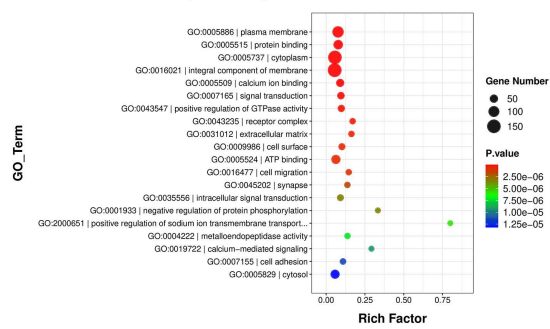
c



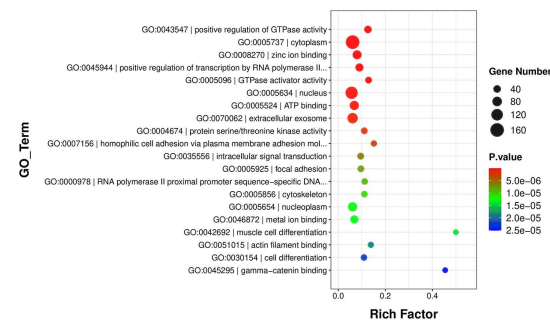
d



(MUSC-1) GO Enrichment ScatterPlot



(MUSC-2) GO Enrichment ScatterPlot



(MUSC-3) GO Enrichment ScatterPlot

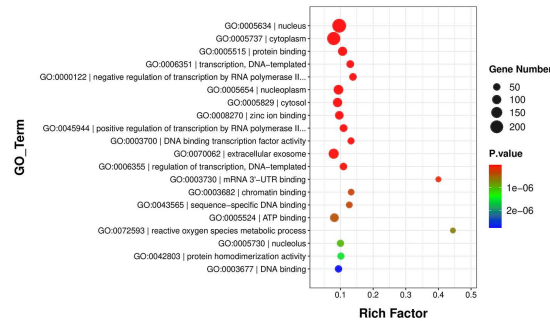


Fig 2. SnRNA-seq analysis showing the expression levels of different genes in MuSCs extracted from the embryonic breast muscle of goose. (a) t-SNE map showing MUSC subgroups. (b) The proportion of MUSC subgroups at E15, E21, and E31 developmental stages. (c) Heat map showing the top 10 upregulated genes in each subgroup of MuSCs. (d) GO functional diagram showing MuSCs subgroups.

<https://doi.org/10.1371/journal.pone.0338390.g002>

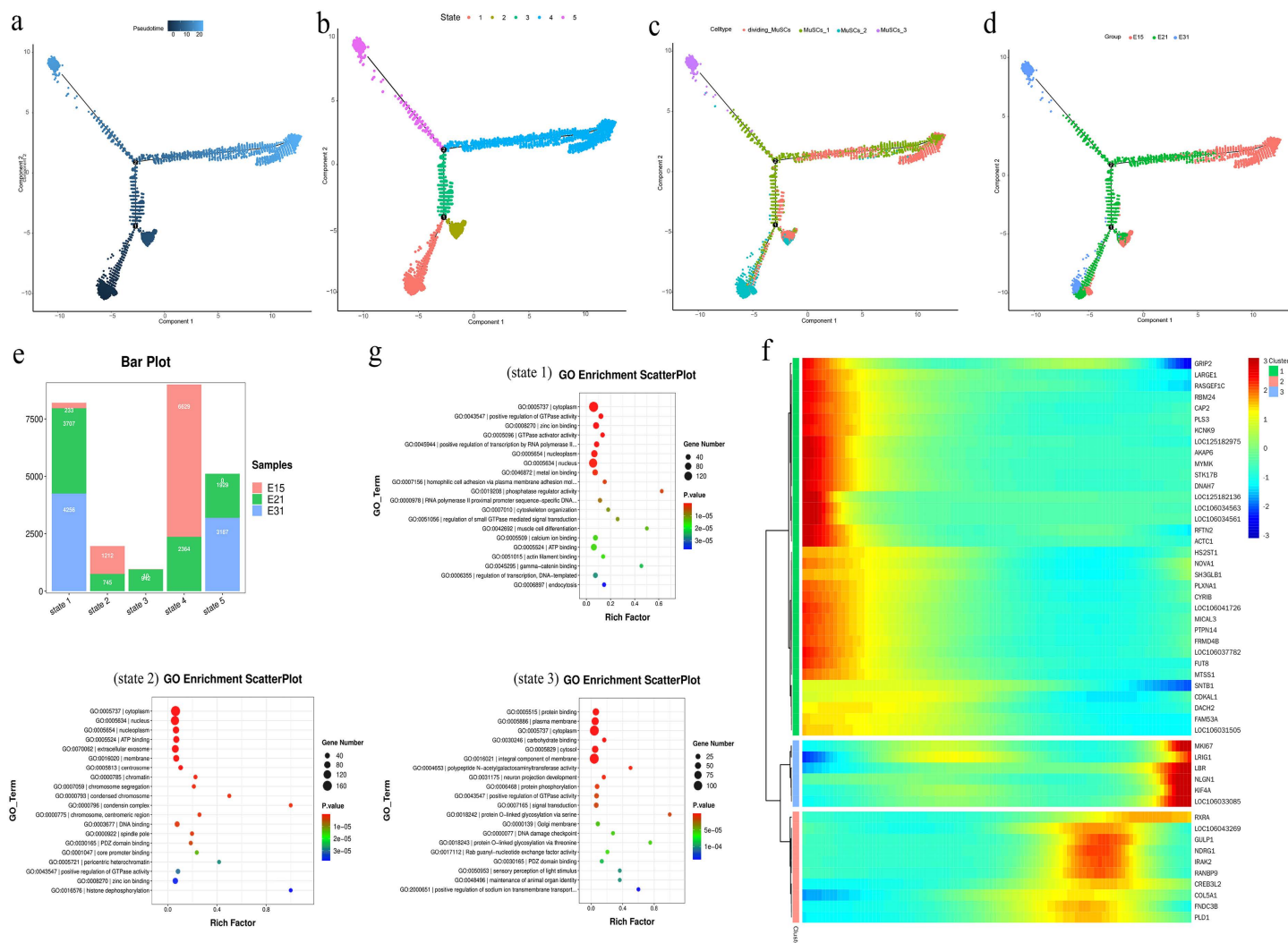


Fig 3. Pseudo-time analysis of the differentiation trajectory of MUSC subgroups. (a) Pseudo-time analysis of individual MuSCs subgroups. (b) Pseudo-time analysis of individual MuSCs subgroups. (c) Pseudo-time analysis based on MuSCs subgroups. (d) Pseudo-time analysis of MUSC subgroups based on three developmental stages. (e) The distribution of five states in three developmental stages. (f) Gene expression heatmap showing pseudo-temporal tree branches. (g) GO enrichment map corresponding to the fate of each cell.

<https://doi.org/10.1371/journal.pone.0338390.g003>

cytoplasm, and was associated with adhesion, metabolism, and MAPK signaling pathways. Of these, *FOXO3*, *PLXDC2*, and *ABLIM1* were specifically expressed, and muscle cell-like FAPs exhibited the characteristics of muscle cells. Next, we compared the proportion of cells at different developmental stages in each cluster (Fig 4e). FAPs-1 accounted for the highest proportion at stage E15, FAPs-2 accounted for the highest proportion at E21, and muscle cell-like FAPs accounted for the highest proportion at E31.

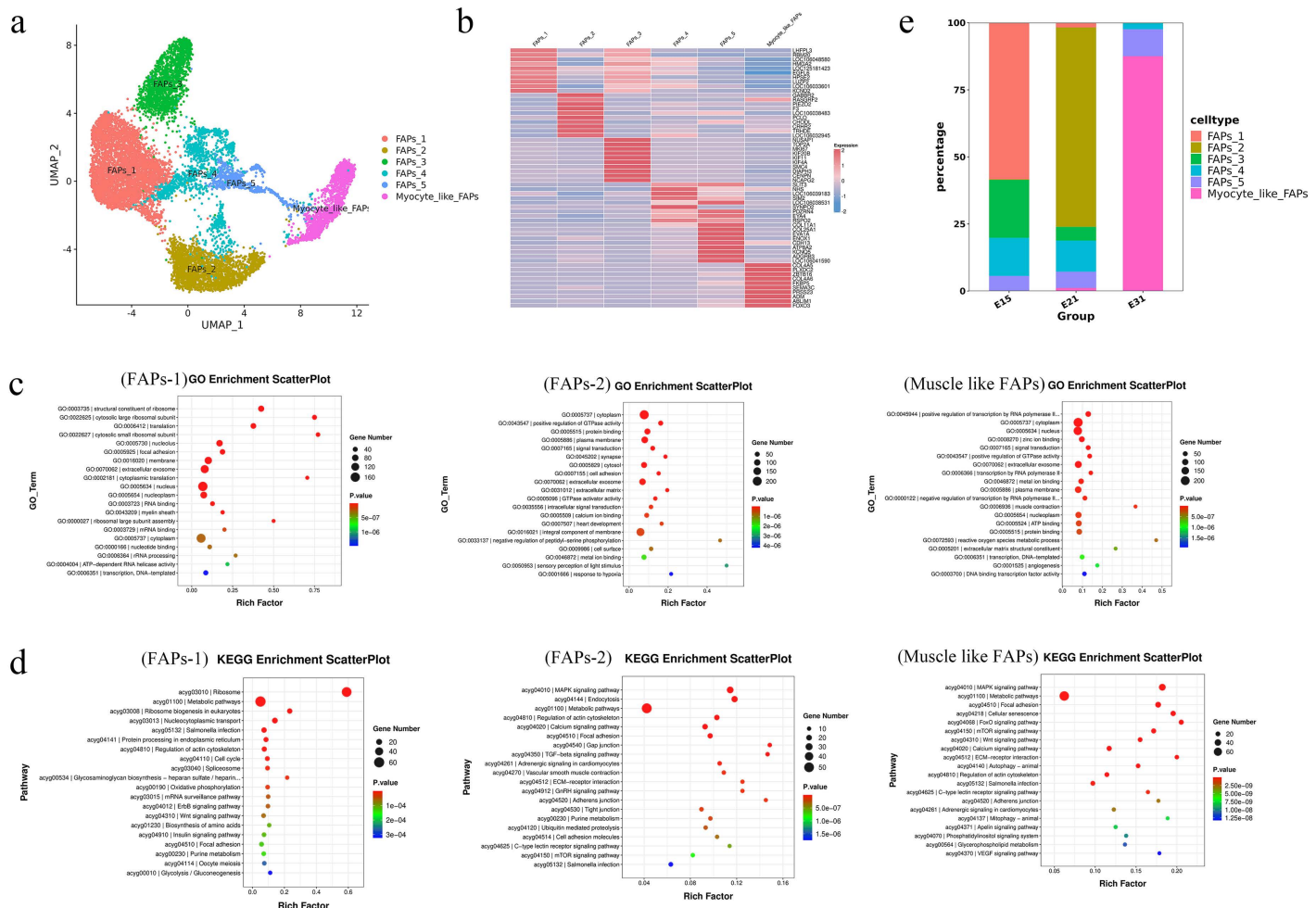


Fig 4. SnRNA-seq analysis showing the expression patterns of different genes in FAPs. (a) t-SNE map showing subgroups of FAPs. (b) Heatmap showing the top ten upregulated genes in the identified FAPs subgroups. (c) GO enrichment in different FAPs subgroups. (d) KEGG analysis of different FAPs subgroups. (e) The proportion of FAPs subgroups in three key developmental stages.

<https://doi.org/10.1371/journal.pone.0338390.g004>

3.5. Typing of myocytes during embryonic development

Myocytes were divided into 12 clusters, and further analysis revealed that these cell clusters exhibited the characteristics of five main cell types (Fig 5a), including neuromuscular junctions (NJs), tendon junctions (MJs), type I fibers, type IIa fibers, and type IIb fibers. As shown in Fig 5b, NJs expressed *ACHE* and *ETV5*; type I fibers expressed *TNNC1*, *ATP2A2*, *TNNI1*, *MYL10*, and *MYH7B*; type II-1 fibers expressed *LRCH1*, *CNKS2*, *B3GALT1*, *JAKMIP1*, *TPM1*, and *TNNC2*; and type II-2 fibers expressed *FOXO3*, *FKBP5*, *RAPGEF5*, *TSPAN18*, and *TNNT3*. Next, we conducted functional enrichment analysis on type I fibers, type II-1 fibers, and type II-2 fibers (Fig 5c). The genes upregulated in type I fibers and II-1 fibers were mainly associated with metabolism, and the MAPK and Wnt signaling pathways. The genes enriched in type II-2 fibers were mainly associated with signaling pathways such as metabolism and purine metabolism. Of these three developmental stages (5d), type IIa fibers accounted for the highest proportion at E15 and E21 (75% and 85%, respectively), while type IIb fibers accounted for the highest proportion at E31 (90%).

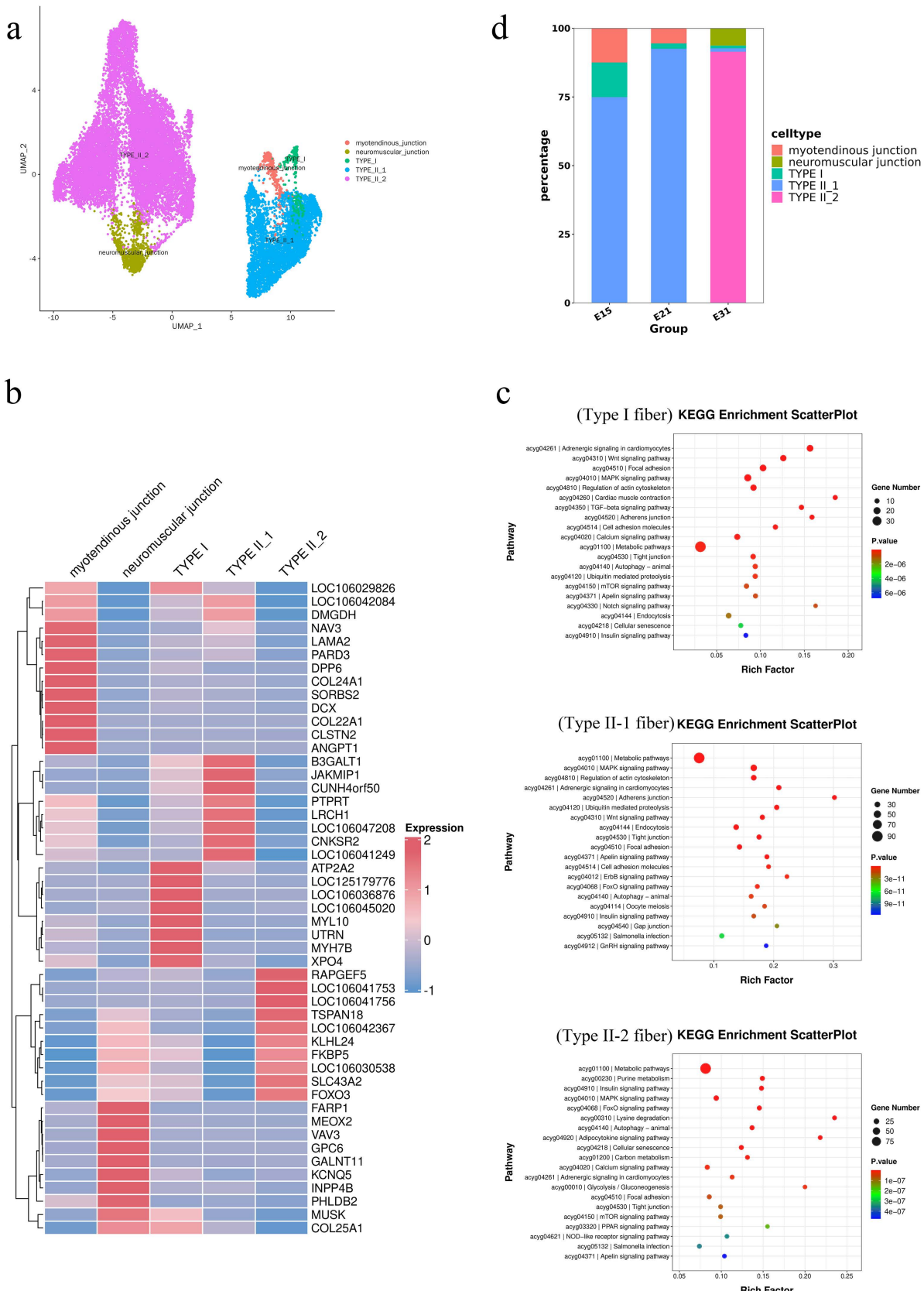


Fig 5. SnRNA-seq analysis showing the expression patterns of different genes in myocytes. (a) t-SNE map showing sub-populations of muscle cells. (b) Heatmap showing the top ten upregulated genes in the sub-populations of muscle cells. (c) KEGG analysis of differentially expressed genes in different subgroups of muscle cells. (d) Proportions of muscle cell sub-populations in three key developmental stages.

<https://doi.org/10.1371/journal.pone.0338390.g005>

3.6. Breast muscle gene regulatory network dynamics

To investigate the differences in transcriptional regulation during breast muscle development, we next analyzed changes in the transcriptional profile of MuSCs, FAPs, and myocytes. Analysis revealed that there were differences in the number of DEGs among the three cell types on E15, E21, and E31 (Fig 6a). E15 vs E31 had the largest DEGs number. Moreover, when analyzed across three time points, we found that the expression levels of *Pax7*, *SIX4*, *Mdm4*, *Id*, and *SIX4* decreased in MUSC, whereas the expression of *Myf5* was upregulated. Notably, the expression of *MEF2* reached its peak at E21 (Fig 6b). In FAPs, a reduction in *Pax7* expression was observed, accompanied by an upregulation of *PDGFRA*, *CD34*, and *IGF1* (Fig 6c). In myocytes, the expression levels of *MyoD*, *Mybpc*, and *Actn* were elevated, while *MSTN* expression was reduced (Fig 6d). Finally, we noticed that *ACTN2*, *MYBPC1*, *TNNT3*, and *LDB3* were significantly downregulated in MuSCs and FAPs ($P < 0.01$), and significantly upregulated ($P < 0.01$) in myocytes during the three developmental stages (Fig 6e).

4. Discussion

This study reports three key novel findings on embryonic breast muscle development in Ding'an goose. Muscle stem cells (MuSCs) can be subdivided into four functionally distinct subpopulations, MUSC-0 (proliferative, expressing TOP2A/MKI67), MUSC-1 (migratory, expressing MMP16/LAMA4), MUSC-2 (transcriptionally regulatory, expressing SOX13/TEAD4), and MUSC-3 (transcription factor-active, expressing ZBTB16/FOXO3)—which sequentially dominate

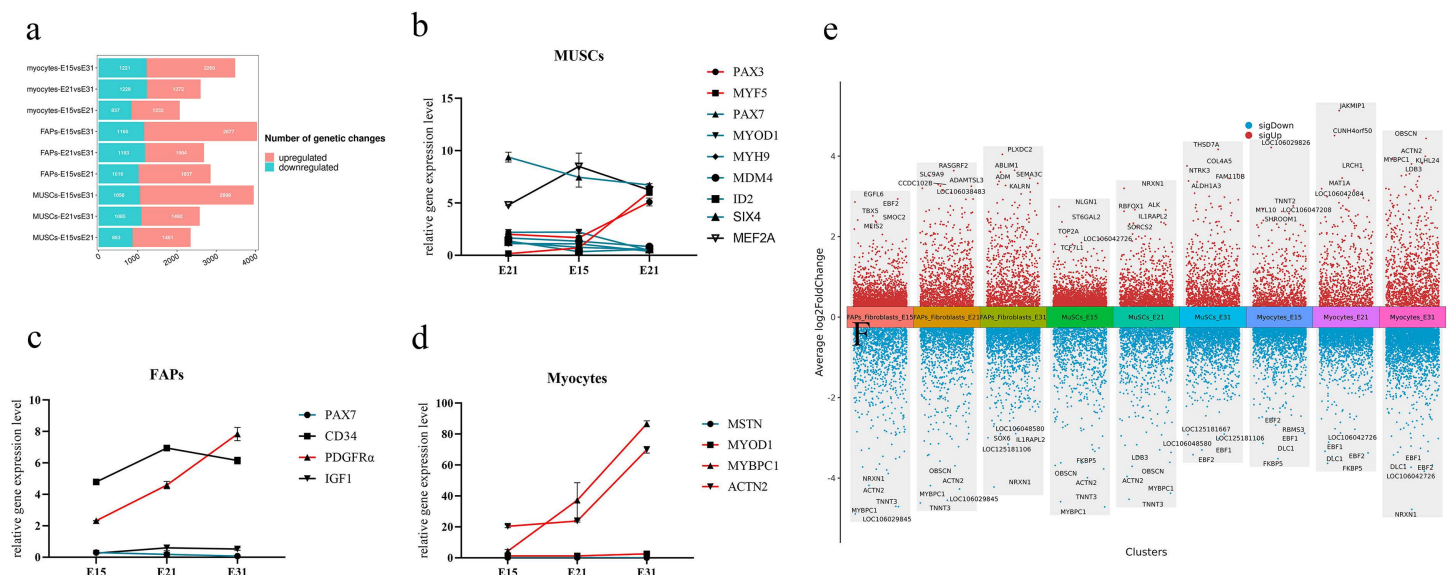


Fig 6. Expression levels of muscle cell genes in breast muscle during the embryonic development of goose. (a) The number of DEGs in myocytes at E15, E21, and E31 stages. (b) DEGs correlated with changes in the proportion of MUSC. (c) DEGs correlated with changes in the proportion of fibro-adipogenic progenitors (FAPs). (d) DEGs correlated with changes in the proportion of myocytes. (e) DEGs associated with breast muscle development.

<https://doi.org/10.1371/journal.pone.0338390.g006>

early, middle, and late developmental stages. (Fibroblast adipogenic progenitor cells (FAPs) differentiate into a unique 'muscle cell-like FAP' subpopulation (expressing FOXO3/PLXDC2/ABLIM1) that becomes the dominant FAP subtype at E31, potentially participating in muscle fiber maturation. Myocytes undergo a subtype transition from Type IIa fiber dominance (E15-E21) to Type IIb fiber dominance (E31), which may underlie the breed's high lean meat rate. These findings collectively delineate the cellular and molecular dynamics specific to Ding'an goose embryonic breast muscle development.

In the present study, we systematically explored the cellular heterogeneity and transcriptional characteristics of skeletal muscle at the single cell level from different aspects in Ding'an goose at E15, E21, and E31 for the first time. Nine cell types were identified in the breast muscle of goose, including myocytes, MuSCs, FAPs/fibroblasts, ECs, SCs, pericytes, IC, RBC, and MSCs. These findings are similar to the SnRNA-seq analysis of mouse breast muscle, as described previously [31]. Early developmental MuSCs accounted for the largest proportion of cell types, while the proportion of myocytes gradually increased during the course of development, accounting for the largest proportion (70%) at E31. Similar to previous study [32] in mice, MuSCs were activated and proliferated during breast muscle development in goose. Some cells retained their MUSC identity, while others differentiated into further dividing myoblasts, which further differentiated into myocytes. More importantly, we observed significant differences in the proportions of identified cell types, including MuSCs, FAPs/fibroblasts, and myocytes at different time points. These results suggest that cell types are relatively stable during this period, and that breast muscle function remains in a dynamic state of change.

Previous study has indicated that MuSCs exhibit high level of heterogeneity during the development of breast muscle [32]. In this study, we identified four MuSCs cell sub-types (MUSC-0, MUSC-1, MUSC-2, MUSC-3) and investigated their unique transcriptome profiles and corresponding functional characteristics. In the MUSC-0, we found that *TOP2A*, *MKI67*, and *CEMNP* were expressed at high levels. Research shows that these genes are known to be significantly associated with cell cycle processes and DNA replication [33–35]. Therefore, we infer that this cell sub-types represents a group of proliferating MuSCs. In the MUSC-1, we found that the *MMP16*, *LAMA4*, and *SRGAP1* were highly expressed, these genes are associated with cell migration [36–39]. Thus, it is possible that MUSC-1 may be related to cell migration and signal transduction. The MUSC-3 specifically expressed *ZBTB16*, *FOXO3* and *COL4A5*, these genes may affect the development of embryonic breast muscle in goose by regulating the synthesis of transcription enzymes [40,41]. In summary, different cell sub-types of MuSCs develop distinct function in breast muscle development.

Pseudo-time analysis is a research method that allows for the recognition and prediction of cell development trajectories [42]. In the present study, we used pseudo-time analysis to investigate the developmental trajectory of embryonic MuSCs in goose. We found that DEGs in different states exhibit dynamic expression patterns and were during the pseudotemporal differentiation process, suggesting their potential involvement in this process. The MUSC-0 plays a role in the early stages of embryonic development, while the MUSC-1, MUSC-2, and MUSC-3 play roles in the middle and late stages of development. The genes were highly expressed in States 1 and 2, and enriched in the cytoplasm and nucleus, while those in State 3 were associated with the overall composition of the cytoplasm and membrane. These results indicated that the metabolism of the MuSCs was enhanced, thereby supporting the growth and development of embryonic breast muscle in goose.

It is well-established that Fibroblast/adipocyte progenitor cells (FAPs) play an important role in muscle regeneration, the maintenance of homeostasis, injury response, and their relationship with adipose tissue [43]. Our analysis confirmed that the main cell sub-types of FAPs were FAPs-1, FAPs-2, FAPs-3, FAPs-4, FAPs-5, and muscle cell-like FAPs. Muscle cell-like FAPs specifically express *FOXO3*, *PLXDC2*, and *ABLIM1*, which are known to be associated with cell migration and cytoskeleton dynamics [44,45]. This may explain the proportion of muscle cell-like FAPs in the majority of cells during late embryonic development. Muscle fiber subtype is a core determinant of poultry meat quality. Type I and Type IIa fibers (slow-twitch fibers) rely on aerobic metabolism, which is associated with bright meat color, small fiber diameter, and high

tenderness. Type IIb fibers (fast-twitch fibers) mainly use glycolytic metabolism, contributing to high lean meat content [46,47]. Ding'an goose is a local breed in Hainan Province known for its high lean meat rate (~75% in breast muscle) and good tenderness [20]. Our results show that Type IIb fibers become the dominant subtype at E31 (90%), which is likely a key cellular basis for its high lean meat trait. Additionally, the maintenance of low but stable Type I fibers (<5%) and the gradual transition from Type IIa to Type IIb fibers may explain the good tenderness of Ding'an goose meat. Previous studies on goose have confirmed that moderate Type IIb fiber proportions avoid tough meat texture, which is consistent with consumer preferences for Ding'an goose [48]. This link between embryonic muscle fiber development and adult meat quality provides a targeted direction for optimizing Ding'an goose genetic breeding.

The development of breast muscle is the result of the synergistic effect of multiple cells [49]. Research has found that *Pax3* is associated with the transformation of muscle cells into limb muscles, and the inactivation of *Pax3* leads to the loss of the limb muscle system [50]. *Myf5* is the first activated muscle regulatory factor, and the inactivation of the *Myf5* gene leads to delayed formation of myotubes [51]. In this study, we found that the expression levels of *Myf5* and *Pax3* increased in MuSCs. Therefore, we speculate that *Myf5* and *Pax3* promote the transition of MuSCs to Myocytes during development. *Pax7* is involved in muscle regeneration and repair [52], *Mdm4* expression helps maintain the proliferation ability of MuSCs to support muscle regeneration [53], and *SIX4* inhibits the activation of slow muscle genes [54]. We found that the expression of *Pax7*, *Mdm4*, and *SIX4* were decreased during development, which inhibiting the formation of MuSCs. This is consistent with the previous findings that the proportion of MuSCs decreases during embryonic development. *Pax7* and *PDGFRa* are involved in regulating the proliferation and differentiation of FAPs [55]. Our findings revealed a downregulation of *Pax7* expression, accompanied by an upregulation of *PDGFRa* expression. *PDGFRa* may decrease the proportion of FAPs by inhibiting their proliferation. Research has found that *MyoD1* can induce multiple cell types to differentiate into Myocytes [56], *Mybpc* is involved in regulating muscle contraction efficiency [57], and *Actn* is involved in maintaining the skeletal structure and stability of Myocytes [58]. We found an increase in the expression of *MyoD*, *Mybpc*, and *Actn* in Myocytes. These genes promoted the transition of other cells to Myocytes, maintained the stability of Myocytes structure and function, and gradually made Myocytes occupy the largest proportion (70%) during development. It is noteworthy that biallelic pathogenic variants in *TNNT3* are associated with congenital myopathies [59], different splice isoforms of the *LDB3* have significant effects on chicken muscle atrophy and sarcomere formation [60], *MYBPC1* knockout mice exhibit impaired skeletal muscle formation and structure after birth [61], and *ACTN2* plays a pivotal role in muscle tissue and myopathies [62]. We found that *ACTN2*, *MYBPC1*, *TNNT3*, and *LDB3* were significantly downregulated in MUSC and FAP, while they were significantly upregulated in myocytes. These analyses revealed that DEGs that involved in regulating the growth and development of skeletal muscles in goose can serve as candidate genes related to the regulation of muscle growth and development in Ding'an goose.

This study has several limitations that should be noted. First, the snRNA-seq technology used in this study only captures nuclear transcriptomes, which may miss mRNAs highly enriched in the cytoplasm. This may lead to incomplete characterization of gene expression profiles in breast muscle cells. Future studies could combine single-cell RNA-seq (scRNA-seq, which captures whole-cell transcriptomes) with snRNA-seq to obtain more comprehensive gene expression information. Second, our analysis focused on three discrete time points (E15, E21, E31); more frequent sampling intervals would help refine the differentiation trajectory of MuSCs and FAPs, potentially identifying transient cell subtypes that play key roles in intermediate developmental stages. Third, we only verified the expression of key DEGs via qPCR and immunofluorescence, but did not validate their functional roles in breast muscle development. Such functional validation would further confirm the causal relationship between DEGs and cell fate decisions. Despite these limitations, the single-cell nucleus transcriptomic atlas of Ding'an goose embryonic breast muscle constructed in this study still provides a foundational resource for understanding the molecular mechanisms of goose breast muscle development.

Conclusions

In summary, this study is the first to construct a single-cell nucleus transcriptomic atlas of breast muscle development in Ding'an goose embryos, revealing the heterogeneity of myoblasts, myocytes, and FAPs. This provides a comprehensive resource for understanding the characteristics, functions, and intercellular interactions of breast muscle cells in Ding'an goose. Additionally, we investigated differences in cell proportions and gene expression levels at the cellular level during key development stages (E15, E21, and E31) to reveal dynamic changes in cell composition and functionality during embryonic development, thus helping us to further understand the molecular mechanisms underlying breast muscle development in Ding'an goose.

Supporting information

S1 Table. snRNA Sequencing Metadata with Pseudotime Analysis for Goose Skeletal Muscle Cells.
(XLSX)

Author contributions

Conceptualization: Tieshan Xu.

Data curation: Yingxiu Hu.

Formal analysis: Xinli Zheng.

Investigation: Qicheng Jiang.

Methodology: Tieshan Xu, Lihong Gu.

Resources: Jie Li, Zhemin Lin.

Software: Lizhi Lu.

Supervision: Tieshan Xu, Lihong Gu.

Validation: Xinli Zheng.

Writing – original draft: Haokai Fan.

Writing – review & editing: Yingxiu Hu.

References

1. Kui H, Ran B, Yang M, Shi X, Luo Y, Wang Y, et al. Gene expression profiles of specific chicken skeletal muscles. *Sci Data*. 2022;9(1):552. <https://doi.org/10.1388/s41597-022-01668-w> PMID: 36075978
2. Shi H, He Y, Li X, Du Y, Zhao J, Ge C. Regulation of Non-Coding RNA in the Growth and Development of Skeletal Muscle in Domestic Chickens. *Genes (Basel)*. 2022;13(6):1033. <https://doi.org/10.3390/genes13061033> PMID: 35741795
3. Persson PB. Skeletal muscle satellite cells as myogenic progenitors for muscle homoeostasis, growth, regeneration and repair. *Acta Physiol (Oxf)*. 2015;213(3):537–8. <https://doi.org/10.1111/apha.12451> PMID: 25565243
4. Sinacore DR, Gulve EA. The role of skeletal muscle in glucose transport, glucose homeostasis, and insulin resistance: implications for physical therapy. *Phys Ther*. 1993;73(12):878–91. <https://doi.org/10.1093/ptj/73.12.878> PMID: 8248296
5. Gu S, Huang Q, Sun C, Wen C, Yang N. Transcriptomic and epigenomic insights into pectoral muscle fiber formation at the late embryonic development in pure chicken lines. *Poult Sci*. 2024;103(8):103882. <https://doi.org/10.1016/j.psj.2024.103882> PMID: 38833745
6. Owens NDL, De Domenico E, Gilchrist MJ. An RNA-Seq Protocol for Differential Expression Analysis. *Cold Spring Harb Protoc*. 2019;2019(6):10.1101/pdb.prot098368. <https://doi.org/10.1101/pdb.prot098368> PMID: 30952685
7. Song X, Li T, Xiong X, Shan H, Feng T, Cui K, et al. RNA-Seq Reveals the Underlying Molecular Mechanism of First Cleavage Time Affecting Porcine Embryo Development. *Genes (Basel)*. 2022;13(7):1251. <https://doi.org/10.3390/genes13071251> PMID: 35886034
8. Kim JL, Jung KM, Han JY. Single-cell RNA sequencing reveals surface markers of primordial germ cells in chicken and zebra finch. *Mol Genet Genomics*. 2024;299(1):90. <https://doi.org/10.1007/s00438-024-02186-7> PMID: 39325237

9. Xu L-K, Ma C-Y, Zhang F-Y, Wang W, Zhao M, Jin X, et al. Embryonic Genome Activation (EGA) Occurred at 1-Cell Stage of Embryonic Development in the Mud Crab, *Scylla paramamosain*, Revealed by RNA-Seq. *Mar Biotechnol (NY)*. 2024;26(6):1246–59. <https://doi.org/10.1007/s10126-024-10369-x> PMID: 39249630
10. Wang Z, Tian W, Wang D, Guo Y, Cheng Z, Zhang Y, et al. Comparative analyses of dynamic transcriptome profiles highlight key response genes and dominant isoforms for muscle development and growth in chicken. *Genet Sel Evol*. 2023;55(1):73. <https://doi.org/10.1186/s12711-023-00849-4> PMID: 37872550
11. Hu Z, Liu X. Integration of Transcriptomics and Non-Targeted Metabolomics Reveals the Underlying Mechanism of Skeletal Muscle Development in Duck during Embryonic Stage. *Int J Mol Sci*. 2023;24(6):5214. <https://doi.org/10.3390/ijms24065214> PMID: 36982289
12. Qu H-Q, Kao C, Hakonarson H. Single-Cell RNA Sequencing Technology Landscape in 2023. *Stem Cells*. 2024;42(1):1–12. <https://doi.org/10.1093/stmcls/sxad077> PMID: 37934608
13. Wang S, Sun S-T, Zhang X-Y, Ding H-R, Yuan Y, He J-J, et al. The Evolution of Single-Cell RNA Sequencing Technology and Application: Progress and Perspectives. *Int J Mol Sci*. 2023;24(3):2943. <https://doi.org/10.3390/ijms24032943> PMID: 36769267
14. Oh J-M, An M, Son D-S, Choi J, Cho YB, Yoo CE, et al. Comparison of cell type distribution between single-cell and single-nucleus RNA sequencing: enrichment of adherent cell types in single-nucleus RNA sequencing. *Exp Mol Med*. 2022;54(12):2128–34. <https://doi.org/10.1038/s12276-022-00892-z> PMID: 36460793
15. Yi C, Song H, Liang H, Ran Y, Tang J, Chen E, et al. TBX3 reciprocally controls key trophoblast lineage decisions in villi during human placenta development in the first trimester. *Int J Biol Macromol*. 2024;263(Pt 1):130220. <https://doi.org/10.1016/j.ijbiomac.2024.130220> PMID: 38368983
16. Marsh B, Blelloch R. Single nuclei RNA-seq of mouse placental labyrinth development. *Elife*. 2020;9:e60266. <https://doi.org/10.7554/elife.60266> PMID: 33141023
17. Wang H, Liu J, Zhu P, Shi L, Liu Y, Yang X, et al. Single-nucleus transcriptome reveals cell dynamic response of liver during the late chick embryonic development. *Poult Sci*. 2024;103(9):103979. <https://doi.org/10.1016/j.psj.2024.103979> PMID: 38941785
18. Hu X, Liu Y, Tang B, Hu J, He H, Liu H, et al. Comparative transcriptomic analysis revealed potential mechanisms regulating the hypertrophy of goose pectoral muscles. *Poult Sci*. 2024;103(12):104498. <https://doi.org/10.1016/j.psj.2024.104498> PMID: 39504833
19. Shi K, Zhou X, Dai J, Gao Y, Gao L, Shen Y, et al. Integrative Transcriptomic and Metabolomic Analysis of Muscle and Liver Reveals Key Molecular Pathways Influencing Growth Traits in Zhedong White Geese. *Animals (Basel)*. 2025;15(9):1341. <https://doi.org/10.3390/ani15091341> PMID: 40362156
20. Xu T, Xu Z, Lu L, Zeng T, Gu L, Huang Y, et al. Transcriptome-wide study revealed m6A regulation of embryonic muscle development in Dingan goose (*Anser cygnoides orientalis*). *BMC Genomics*. 2021;22(1):270. <https://doi.org/10.1186/s12864-021-07556-8> PMID: 33853538
21. Zheng GXY, Terry JM, Belgrader P, Ryvkin P, Bent ZW, Wilson R, et al. Massively parallel digital transcriptional profiling of single cells. *Nat Commun*. 2017;8:14049. <https://doi.org/10.1038/ncomms14049> PMID: 28091601
22. Butler A, Hoffman P, Smibert P, Papalexi E, Satija R. Integrating single-cell transcriptomic data across different conditions, technologies, and species. *Nat Biotechnol*. 2018;36(5):411–20. <https://doi.org/10.1038/nbt.4096> PMID: 29608179
23. Sun J, Philpott M, Loi D, Li S, Monteagudo-Mesas P, Hoffman G, et al. Correcting PCR amplification errors in unique molecular identifiers to generate accurate numbers of sequencing molecules. *Nat Methods*. 2024;21(3):401–5. <https://doi.org/10.1038/s41592-024-02168-y> PMID: 38317008
24. Luecken MD, Theis FJ. Current best practices in single-cell RNA-seq analysis: a tutorial. *Mol Syst Biol*. 2019;15(6):e8746. <https://doi.org/10.15252/msb.2018746> PMID: 31217225
25. Hao Y, Stuart T, Kowalski MH, Choudhary S, Hoffman P, Hartman A, et al. Dictionary learning for integrative, multimodal and scalable single-cell analysis. *Nat Biotechnol*. 2024;42(2):293–304. <https://doi.org/10.1038/s41587-023-01767-y> PMID: 37231261
26. Li J, Yang D, Chen C, Wang J, Wang Z, Yang C, et al. Single-cell RNA transcriptome uncovers distinct developmental trajectories in the embryonic skeletal muscle of Daheng broiler and Tibetan chicken. *BMC Genomics*. 2025;26(1):187. <https://doi.org/10.1186/s12864-025-11363-w> PMID: 39994525
27. Bai X, Cao J, Dong Y, Wang Z, Chen Y. Melatonin mediates monochromatic green light-induced satellite cell proliferation and muscle growth in chick embryo. *PLoS One*. 2019;14(5):e0216392. <https://doi.org/10.1371/journal.pone.0216392> PMID: 31059537
28. Yablonka-Reuveni Z, Day K, Vine A, Shefer G. Defining the transcriptional signature of skeletal muscle stem cells. *J Anim Sci*. 2008;86(14 Suppl):E207-16. <https://doi.org/10.2527/jas.2007-0473> PMID: 17878281
29. Nascimento CS, Barbosa LT, Brito C, Fernandes RPM, Mann RS, Pinto APG, et al. Identification of Suitable Reference Genes for Real Time Quantitative Polymerase Chain Reaction Assays on Pectoralis major Muscle in Chicken (*Gallus gallus*). *PLoS One*. 2015;10(5):e0127935. <https://doi.org/10.1371/journal.pone.0127935> PMID: 26020643
30. Hu Y-X, Liang Q, Li A, Bai D-P. Mechanism of fatty acid transposase (CD36) promoting fat accumulation in mule ducks. *Poult Sci*. 2024;103(12):104268. <https://doi.org/10.1016/j.psj.2024.104268> PMID: 39260245
31. Petranay MJ, Swoboda CO, Sun C, Chetal K, Chen X, Weirauch MT, et al. Single-nucleus RNA-seq identifies transcriptional heterogeneity in multi-nucleated skeletal myofibers. *Nat Commun*. 2020;11(1):6374. <https://doi.org/10.1038/s41467-020-20063-w> PMID: 33311464
32. Williams K, Yokomori K, Mortazavi A. Heterogeneous Skeletal Muscle Cell and Nucleus Populations Identified by Single-Cell and Single-Nucleus Resolution Transcriptome Assays. *Front Genet*. 2022;13:835099. <https://doi.org/10.3389/fgene.2022.835099> PMID: 35646075

33. Guilhot C, Catenacci M, Lofaro S, Rudnicki MA. The satellite cell in skeletal muscle: A story of heterogeneity. *Curr Top Dev Biol.* 2024;158:15–51. <https://doi.org/10.1016/bs.ctdb.2024.01.018> PMID: 38670703
34. Duan Y, Fu H, Huang J, Yin N, Liu L, Liu X. TOP2A deficiency leads to human recurrent spontaneous abortion and growth retardation of mouse pre-implantation embryos. *Mol Med.* 2022;28(1):165. <https://doi.org/10.1186/s10020-022-00592-4> PMID: 36585615
35. Wu S-Y, Liao P, Yan L-Y, Zhao Q-Y, Xie Z-Y, Dong J, et al. Correlation of MKI67 with prognosis, immune infiltration, and T cell exhaustion in hepatocellular carcinoma. *BMC Gastroenterol.* 2021;21(1):416. <https://doi.org/10.1186/s12876-021-01984-2> PMID: 34724892
36. Qi C-L, Huang M-L, Zou Y, Yang R, Jiang Y, Sheng J-F, et al. The IRF2/CENP-N/AKT signaling axis promotes proliferation, cell cycling and apoptosis resistance in nasopharyngeal carcinoma cells by increasing aerobic glycolysis. *J Exp Clin Cancer Res.* 2021;40(1):390. <https://doi.org/10.1186/s13046-021-02191-3> PMID: 34893086
37. Yamazaki D, Itoh T, Miki H, Takenawa T. srGAP1 regulates lamellipodial dynamics and cell migratory behavior by modulating Rac1 activity. *Mol Biol Cell.* 2013;24(21):3393–405. <https://doi.org/10.1091/mbc.E13-04-0178> PMID: 24006490
38. Huang X, Ji G, Wu Y, Wan B, Yu L. LAMA4, highly expressed in human hepatocellular carcinoma from Chinese patients, is a novel marker of tumor invasion and metastasis. *J Cancer Res Clin Oncol.* 2008;134(6):705–14. <https://doi.org/10.1007/s00432-007-0342-6> PMID: 18084776
39. Shen Z, Wang X, Yu X, Zhang Y, Qin L. MMP16 promotes tumor metastasis and indicates poor prognosis in hepatocellular carcinoma. *Oncotarget.* 2017;8(42):72197–204. <https://doi.org/10.18632/oncotarget.20060> PMID: 29069779
40. Šeda O, Šedová L, Včelák J, Vaňková M, Liška F, Bendlová B. ZBTB16 and metabolic syndrome: a network perspective. *Physiol Res.* 2017;66(Suppl 3):S357–65. <https://doi.org/10.33549/physiolres.933730> PMID: 28948820
41. Cao G, Lin M, Gu W, Su Z, Duan Y, Song W, et al. The rules and regulatory mechanisms of FOXO3 on inflammation, metabolism, cell death and aging in hosts. *Life Sci.* 2023;328:121877. <https://doi.org/10.1016/j.lfs.2023.121877> PMID: 37352918
42. Shangguan Y, Li C, Lin H, Ou M, Tang D, Dai Y, et al. Application of single-cell RNA sequencing in embryonic development. *Genomics.* 2020;112(6):4547–51. <https://doi.org/10.1016/j.ygeno.2020.08.007> PMID: 32781204
43. Giuliani G, Rosina M, Reggio A. Signaling pathways regulating the fate of fibro/adipogenic progenitors (FAPs) in skeletal muscle regeneration and disease. *FEBS J.* 2022;289(21):6484–517. <https://doi.org/10.1111/febs.16080> PMID: 34143565
44. Narahara H, Sakai E, Yamaguchi Y, Narahara S, Iwatake M, Okamoto K, et al. Actin binding LIM 1 (abLIM1) negatively controls osteoclastogenesis by regulating cell migration and fusion. *J Cell Physiol.* 2018;234(1):486–99. <https://doi.org/10.1002/jcp.26605> PMID: 29904924
45. Miller-Delaney SFC, Lieberam I, Murphy P, Mitchell KJ. Plxdc2 is a mitogen for neural progenitors. *PLoS One.* 2011;6(1):e14565. <https://doi.org/10.1371/journal.pone.0014565> PMID: 21283688
46. Zhang D, Xu F, Liu Y. Research progress on regulating factors of muscle fiber heterogeneity in poultry: a review. *Poult Sci.* 2024;103(9):104031. <https://doi.org/10.1016/j.psj.2024.104031> PMID: 39033575
47. Wang H, Shen Z, Zhou X, Yang S, Yan F, He K, et al. Identification of differentially expressed genes in different types of broiler skeletal muscle fibers using the RNA-seq technique. *Biomed Res Int.* 2020;2020:9478949. <https://doi.org/10.1155/2020/9478949> PMID: 32695825
48. Mo M, Zhang Z, Wang X, Shen W, Zhang L, Lin S. Molecular mechanisms underlying the impact of muscle fiber types on meat quality in livestock and poultry. *Front Vet Sci.* 2023;10:1284551. <https://doi.org/10.3389/fvets.2023.1284551> PMID: 38076559
49. Abdelmoez AM, Sardón Puig L, Smith JAB, Gabriel BM, Savikj M, Dollet L, et al. Comparative profiling of skeletal muscle models reveals heterogeneity of transcriptome and metabolism. *Am J Physiol Cell Physiol.* 2020;318(3):C615–26. <https://doi.org/10.1152/ajpcell.00540.2019> PMID: 31825657
50. de Morree A, Klein JDD, Gan Q, Farup J, Urtasun A, Kanugovi A, et al. Alternative polyadenylation of Pax3 controls muscle stem cell fate and muscle function. *Science.* 2019;366(6466):734–8. <https://doi.org/10.1126/science.aax1694> PMID: 31699935
51. Lindon C, Montarras D, Pinset C. Cell cycle-regulated expression of the muscle determination factor Myf5 in proliferating myoblasts. *J Cell Biol.* 1998;140(1):111–8. <https://doi.org/10.1083/jcb.140.1.111> PMID: 9425159
52. Song R, Zhao S, Xu Y, Hu J, Ke S, Li F, et al. MRTF-A regulates myoblast commitment to differentiation by targeting PAX7 during muscle regeneration. *J Cell Mol Med.* 2021;25(18):8645–61. <https://doi.org/10.1111/jcmm.16820> PMID: 34347392
53. Wang P, Liu X, Yao Z, Chen Y, Luo L, Liang K, et al. Lin28a maintains a subset of adult muscle stem cells in an embryonic-like state. *Cell Res.* 2023;33(9):712–26. <https://doi.org/10.1038/s41422-023-00818-y> PMID: 37188880
54. Yajima H, Motohashi N, Ono Y, Sato S, Ikeda K, Masuda S, et al. Six family genes control the proliferation and differentiation of muscle satellite cells. *Exp Cell Res.* 2010;316(17):2932–44. <https://doi.org/10.1016/j.yexcr.2010.08.001> PMID: 20696153
55. Tseng H-W, Girard D, Alexander KA, Millard SM, Torossian F, Anginot A, et al. Spinal cord injury reprograms muscle fibroadipogenic progenitors to form heterotopic bones within muscles. *Bone Res.* 2022;10(1):22. <https://doi.org/10.1038/s41413-022-00188-y> PMID: 35217633
56. Yang Z, MacQuarrie KL, Analau E, Tyler AE, Dilworth FJ, Cao Y, et al. MyoD and E-protein heterodimers switch rhabdomyosarcoma cells from an arrested myoblast phase to a differentiated state. *Genes Dev.* 2009;23(6):694–707. <https://doi.org/10.1101/gad.1765109> PMID: 19299559
57. Harris SP. Making waves: A proposed new role for myosin-binding protein C in regulating oscillatory contractions in vertebrate striated muscle. *J Gen Physiol.* 2021;153(3):e202012729. <https://doi.org/10.1085/jgp.202012729> PMID: 33275758
58. Lin W-S, Lu K-M, Chung M-H, Liu S-T, Chen H-H, Chang Y-L, et al. The subcellular localization and protein stability of mouse alpha-actinin 2 is controlled by its nuclear receptor binding motif in C2C12 cells. *Int J Biochem Cell Biol.* 2010;42(12):2082–91. <https://doi.org/10.1016/j.biocel.2010.09.024> PMID: 20933605

59. Calame DG, Fatih J, Herman I, Akdemir ZC, Du H, Jhangiani SN, et al. Biallelic Pathogenic Variants in TNNT3 Associated With Congenital Myopathy. *Neurol Genet*. 2021;7(3):e589. <https://doi.org/10.1212/NXG.0000000000000589> PMID: 33977145
60. Wei C, Niu Y, Chen B, Wang Y, Cai H, Han R, et al. Divergent Regulatory Roles of Transcriptional Variants of the Chicken LDB3 Gene in Muscle Shaping. *J Agric Food Chem*. 2024;72(21):12240–50. <https://doi.org/10.1021/acs.jafc.4c00520> PMID: 38764183
61. Song T, McNamara JW, Ma W, Landim-Vieira M, Lee KH, Martin LA, et al. Fast skeletal myosin-binding protein-C regulates fast skeletal muscle contraction. *Proc Natl Acad Sci U S A*. 2021;118(17):e2003596118. <https://doi.org/10.1073/pnas.2003596118> PMID: 33888578
62. Ranta-aho J, Olivé M, Roticiani G, Vandroux M, Dominguez C, Johari M, et al. VP.68 ACTN2: Mutation Update. *Neuromuscular Disorders*. 2022;32:S112. <https://doi.org/10.1016/j.nmd.2022.07.290>